Single-molecule manipulation and chemistry with the STM

2005 J. Phys.: Condens. Matter 17 S1049

(http://iopscience.iop.org/0953-8984/17/13/003)

INSTITUTE OF PHYSICS PUBLISHING JOURNAL OF PHYSICS: CONDENSED MATTER

J. Phys.: Condens. Matter **17** (2005) S1049–S1074 doi:10.1088/0953-8984/17/13/003

Single-molecule manipulation and chemistry with the STM

N Lorente[1,3], R Rurali[1] and H Tang[2]

[1] Laboratoire Collisions Agrégats et Réactivité, UMR 5589, IRSAMC, Université Paul Sabatier, 118 route de Narbonne, Toulouse, 31062 Cédex, France
[2] CEMES/CNRS, 29, rue Jeanne Marvig, BP 94347, Toulouse, 31055 Cédex, France

E-mail: lorente@irsamc.ups-tlse.fr

Received 2 August 2004, in final form 9 January 2005
Published 18 March 2005
Online at stacks.iop.org/JPhysCM/17/S1049

Abstract

We review recent theoretical work on the manipulation of single molecules with scanning probes, in particular the scanning tunnelling microscope (STM). The aim of theories and simulations is to account for the processes, ideally at a quantitative level, that permit the controlled manipulation of matter at the atomic scale in adsorbed molecular systems. In order to achieve this, simulations rely on total energy and electronic structure calculations where a trade-off is made between the size of the system and the accuracy of the calculation. This first stage of the calculation yields the basic quantities used for the second stage: the evaluation of the coupled electron–nuclear dynamics. This second stage is a formidable task and many approximations are involved. In this review, we will present some of the customary approximations regarding the theoretical study of mechanical and inelastic manipulations. Mechanical manipulations use the interaction between the acting probe (usually a metallic tip) and the targeted adsorbate. We review recent results in the field of adsorbate mechanical manipulations and explain how manipulations can be effected by using the interaction between the probe's tip and certain molecular groups of complex chemisorbed molecular systems. On the other hand, inelastic manipulations use the tunnelling current to convey energy with sub-ångström precision. This current can excite localized vibrations that can induce measurable variations of the tunnelling conductance, hence providing a means of detecting single-molecule vibrations. This current can also inject energy in a few reaction coordinates. Recently, the possibility of vibrational selective manipulations of NH_3/Cu(100) has been experimentally demonstrated. The theory presented here addresses the actual pathways accessed when the molecule is excited by the tunnelling current from an STM.

(Some figures in this article are in colour only in the electronic version)

[3] Author to whom any correspondence should be addressed.

0953-8984/05/131049+26$30.00

1. Introduction

Since the discovery of the scanning tunnelling microscope (STM) [1] the analysis of condensed matter systems in terms of their atomic structure has become a routine activity in surface science laboratories. An STM consists of a metallic tip, a tip manipulator (vertical positioning with a precision down to $\sim$0.01 Å) and sophisticated electronics that record the tip–substrate electron current, bias voltage and manipulator motion. At constant tunnelling current, mapping the set of tip positions along a surface scan yields topographical images that were realized as a major breakthrough: the atomic structure of surfaces became directly measurable. Soon after, other modes of operation of the STM became apparent, together with other scanning probes (notably the atomic force microscope, AFM). In particular, the possibility of inducing motion of atomic adsorbates was demonstrated in the early 1990s [2]. This stirred a lot of activity both experimentally and theoretically; not only could atoms be 'seen', but also they could also be 'touched'. Since then, the STM has become a single-molecule laboratory: it can detect, analyse and modify the adsorbed molecules.

The aim of the present paper is to present a succinct review of the latest advances in the field of single-adsorbate manipulations from a theoretical point of view. There have been excellent related reviews in the last years [3–5]. Here, manipulations will be classified according to their physical principle. Initially, we will review mechanical manipulations where the interaction exerted by the probe's tip on the adsorbate is used to initiate its motion. Secondly, we will review recent work in the modelling and computation of inelastic effects localized at molecular adsorbates. In both cases (mechanical and inelastic manipulations) the scanning probe is used both as the manipulating element and as the detecting element.

Mechanical manipulations with a scanning probe can be divided into two categories according to Stroscio and collaborators [6]: vertical and lateral manipulations. The vertical process is an adsorbate transfer between the tip and the substrate [7, 8]. The adsorbate can then be extracted permanently from the substrate or be re-positioned. In contrast, during a lateral manipulation process, the adsorbate never loses contact with the host surface.

Manipulations can also be effected by using the tip–substrate electrical current. Inelastic effects take place when a current flows through a system where vibrations are possible. Nuclear motion affects the electronic structure, and the converse is also true. Hence the changing occupation of electronic states exerts forces on the nuclei that can eventually lead to vibrational excitation. This has been used to record the vibrational spectra of single molecules on surfaces [10]. In this paper, we summarize the modelling and analysis of the data of STM vibrational spectra, where the molecule is at most excited to its first quantum of vibration. However, the degree of molecular excitation can be increased depending on the energy of and time between impinging electrons. These parameters can be controlled by the tip–substrate voltage bias and current respectively. The tunnelling current has a sub-ångström extension with an extraordinary precision in the location of the exciting electron beam. Typical manipulation parameters have a large range of electron power: from nW to pW.

The combination of the exciting and detecting probes in the STM tip has disadvantages in the difficulty of analysing the signals and the physical processes, but the STM has an extraordinary sensitivity to the detection of reaction products. Reactions induced with the STM can have yields as low as 10^{-10} which are perfectly detectable. Indeed, this is one of the advantages of the STM: it can probe the region of very low power and very low reaction yields, giving information about otherwise inaccessible processes.

Recently, the STM has been used to induce mode specific reactions on NH_3 molecules chemisorbed on Cu(100) [11]. The STM parameters had been tuned to overcome certain molecular barriers by choosing bias voltages that could excite certain molecular modes and by

choosing the current that permits decay of the molecule between exciting electrons. Hence, the excitation of a single N–H stretch mode was identified with the translation of the molecule. When the N–H stretch was not available, the umbrella mode was efficient in desorbing the molecule if several electrons could excite it before de-excitation of the mode by its coupling with the surface degrees of freedom. The analysis of these data has led to the revealing of the role of anharmonicity and enhanced intermode coupling existing at surfaces: the symmetry of the molecule is lowered and the continuum of available electronic excitations permits many processes that would be otherwise forbidden.

In order to achieve quantitative modelling of the manipulation processes of single molecules, an accurate knowledge of electronic structure, condensed matter interactions, electron–vibration couplings, and total energies needs to be achieved. Hence, in the following section we will introduce the reader to the theoretical tools that are routinely used as the basis of molecular modellization. In the third section of the paper, we will present a brief review of mechanical manipulations and the fourth section will be devoted to inelastic effects, their meaning, modelling and recent results. This paper ends with a brief outlook on the field of simulations directed to the evaluation of single-adsorbate manipulation processes.

2. Numerical simulations and theoretical tools

Simulations of molecular manipulation with scanning probes build on calculations of the electron and nuclear ensemble. In order to estimate the forces exerted on the different atomic constituents one needs calculations as accurate as possible of the systems of interest. The simulations including electron–vibration coupling, atom–atom interactions will use the result of total energy calculations. It is then important to have access to a group of numerical and computational tools that permit us to compute the total energy as is most convenient for the system studied. In this section we present a brief review of the total energy techniques that are used to characterize and evaluate different condensed matter systems.

The fundamental theory of condensed matter is well established and the electronic structure problem is very well defined [12]. However, due to the complexity of the equations involved, an exact solution of the many-body Schrödinger equation is not possible, at least not for the size of typical systems of interest [13]. A variety of methods have been developed that allow us to treat approximately the quantum mechanical problem.

A breakthrough among methodological advances is density functional theory (DFT) [14, 15]. Since its first formulation, back in 1964, DFT has encountered growing interest and it is nowadays a standard in computational materials science, especially in solid state physics. DFT provides a framework in which to understand the basic physics of many-electron systems without the complexity of the many-body wavefunction [16]. The treatment within DFT is formally exact, provided that the functional for the exchange–correlation contribution to the total energy is known: the approximation consists in considering approximated formulations of this functional [17, 18]. Nevertheless, these approximated functionals have been thoroughly tested ever since the development of the theory, giving us a large body of experience as regards what properties and systems can be accurately described. In spite of the apparent crudeness of some of these approximations, they usually perform well. In the solid state physics community, DFT approaches are considered *ab initio* treatments given the absence of parameters once a justified approximated calculation for the exchange and correlation functional has been performed. The most common of these treatments is the local density approximation (LDA) where the exact exchange and correlation functional of a homogeneous electron gas is used, and the homogeneous electron density is taken as the local electron density, i.e. the electronic density at a given point in space. This approximation necessarily breaks down in systems where the electronic density is varying rapidly, such

as molecules and surfaces. Hence approximations taking into account the gradient of the electronic density and the density at a given point in space have been produced and are termed generalized gradient approximations (GGA). In the chemistry community, these approaches are not considered to be at the *ab initio* level. In particular, this last view is correct in certain GGAs that have been parametrized to reproduce several physical parameters of particular systems without any other justification.

The minimization of the approximated energy functional is performed through the Kohn–Sham equations [15]. These equations reduce the electronic DFT problem to a set of independent pseudo-electrons that move in an effective, self-consistent potential. Once that the problem has been mapped into Kohn–Sham form, the exchange and correlation functional gathers in all of the energy functional that has been left out in the process of converting the minimization of the functional into an effective set of Shrödinger-like one-particle equations (the Kohn–Sham equations). In particular, the exchange and correlation functional includes information on the kinetic energy functional since the kinetic energy of the Kohn–Sham equations does not contain all of the kinetic energy functional; it also includes the terms coming from a Hartree–Fock approach of the Kohn–Sham electrons, and everything that is left out of a one-body treatment: the correlation.

In a general application, the Kohn–Sham eigenfunctions are heuristically used as the *true* one-electron wavefunctions. This is not justified, but the success of theories based on this approach is probably based on accounting for several effects in the approximate effective one-particle potential. The most notable failure of DFT is the wrong band gaps obtained from Kohn–Sham eigenenergies. In this case, not only is the use of the Kohn–Sham electronic structure unjustified, but so also is the use of DFT itself because DFT is a ground state theory. In most of the cases however, its reasonable accuracy and its one-body simplicity permits the computation of electronic and nuclear properties of systems large enough (a few hundred atoms depending on the system) to be interesting.

Computationally, the Kohn–Sham one-electron wavefunction is expanded on a convenient basis set. Many well established computer codes [19–21] use a plane wave (PW) basis set. The sum over PW is extended up to a chosen cut-off and by adjusting this single parameter the quality of the basis set can be systematically improved. Neglecting PW beyond a certain cut-off means losing the spatial resolution of the wavefunction for distances below a certain value. The main alternative consists in expanding the eigenstate wavefunctions on a basis set of localized orbitals. The quantum chemistry community regularly use basis sets made up of Gaussian-like orbitals [22, 23], while among solid state physicists, the use of optimized atomic orbital approaches [24, 25] is becoming popular.

Despite the enormous simplification of the many-body problem introduced by DFT, systems over certain sizes are still difficult to treat on the basis of a full *ab initio* approach. A valid alternative is represented by tight binding (TB) methods [26]. In TB, the Hamiltonian is not directly calculated from first principles, but has been previously parametrized on the basis of experimental results or of DFT calculations. Like in DFT, the computational cost associated with solving an electronic structure is $O(N^3)$, i.e. it scales with the cube of the number of atoms, because a matrix diagonalization is still involved. However, in TB the effort required to build the Hamiltonian is orders of magnitude lower, if compared to DFT. Although it relies on a parametrization, in TB the quantum mechanics of bonding is preserved and an electronic structure is still available, albeit an approximate one. The attainable system size is a few thousand atoms. Hence, TB allows a study of systems larger than the ones treated with DFT, at the expense of a lower accuracy and less predictive power.

Moving a step further, one can model atoms as point-like bodies that move inside a potential, often described analytically. In such a framework, electrons are no longer explicitly

taken into account and their effect is only considered by means of a potential inside which the ions move. Modelling a material by an empirical potential brings along a trade-off between accuracy and portability. The need to make an assumption on the spatial distribution of chemical bonds drastically limits the range of compounds for which good performances of the model can be expected. Many of the most well known potentials have been developed for silicon [27–31]. Some of these potentials have been very successful in accurately predicting solid state structures. Such is the case of the Tersoff potential that gives the diamond phase and the graphene structure of carbon [32]. The approach of empirical potentials has been massively extended in the field of biological applications. In this case, due to the complexity of the interactions, force fields [33–35] are used rather than closed-form analytical functions. The system sizes that can be treated range from hundreds of thousands of atoms to a few million atoms.

Unfortunately, parametrization introduces a few problems that can sometimes constitute a serious limiting factor. The most obvious one is that an appropriate parametrization must be available and, if not, worked out. In the case of TB this amounts to parametrizing the hopping elements between the different species and, if one is treating a model involving a non-orthogonal basis, the overlap matrix is also parametrized. With empirical potentials the situation is even more extreme, as typically one has to adapt or even to change the functional form itself, i.e. the Tersoff potential works remarkably well for some of group IV semiconductors, but it probably cannot be extended to take into account interactions with, for instance, copper, without drastically revising it and reformulating it. The main problem of a parametrization is its portability. When parametrizing a TB Hamiltonian with a series of DFT calculations one tries to satisfactorily reproduce certain properties of the system, i.e. the electronic structure, bond lengths, bond angles, lattice parameter and cohesion energies in the case of solids or binding energies in the case of molecules. However, the transferability of potentials and parametrized Hamiltonians to configurations different from those used to build the parametrization is a very delicate issue and has to be carefully investigated.

Once the total energy has been calculated, one can obtain the forces acting on each atom by performing spatial derivatives of the total energy with respect to the atomic coordinates. This information is extremely valuable, because it allows us to evaluate the geometrical evolution of an atomic system. The precision of the calculated forces depends on how accurate the estimation of the energy is. Most typically, these forces are used to achieve the minimum energy structure of a system by varying the atomic coordinates. A standard choice of algorithm for configuration optimization is the *conjugate gradient* method. Alternatively, the computed forces can be used to perform *molecular dynamics* (MD), that is an actual follow-up of the dynamical evolution at a given temperature. The main difference with a minimum energy—or *static*—algorithm is that the atomic energy contains a kinetic component. MD permits one to study transitions—the frequency with which they occur or the energy barrier associated—and to calculate magnitudes that are intrinsic averages over time such as temperature or pressure. However, the time intervals that can be spanned are usually too short to be statistically significant, limiting the use of MD to some specific cases.

Inelastic single-molecule manipulation typically relies on very subtle—often intrinsically quantum mechanical—effects, such as vibrational excitation. For this reason, when the subject of study is the physics of single molecular adsorbates, one reverts to *ab initio* methods. This choice is dictated essentially by the need of obtaining the most accurate estimations of total energy, forces, and eventually derived quantities such as electron–vibration couplings. First-principles-like approaches present the advantage of attaining a given accuracy without an explicit dependence on the existence of a parametrization or on the reliability of the parametrization. Mechanical manipulations, on the other hand, have been successfully

modelled by empirical and semi-empirical methods. The use of approximate methods is generally imposed by the relatively large scale of the systems required to simulate such processes.

3. Mechanical manipulation

In 1990, the first demonstration of individual atom manipulation was performed by Eigler and Schweizer [2], in which individual xenon atoms were picked up by the STM tip and then were re-deposited on a Ni(110) surface. 35 Xe atoms were used to form the acronym 'IBM'. Nowadays, individual-atom/molecule manipulations are routinely effected, even with commercial equipment [36]. However, severe conditions such as UHV or very low temperatures on metal surfaces are necessary to achieve single-adsorbate manipulation capabilities.

Atomic force microscope (AFM) manipulations are currently possible. Yet, due to the AFM difficulties of obtaining atomically resolved images, only large biological molecules or carbon nanotubes have been manipulated [37, 38]. The main obstacle to achieving single-adsorbate manipulations is that the atomic force variation versus the tip–surface distance does not have an exponential decrease like the tunnelling current in the STM. The new atomic resolution of non-contact AFM families (NC-AFM) may render possible the control of individual atomic or molecular objects in vacuum. At present, it has been possible to switch a group conformation in some organic molecules by means of the interaction of a NC-AFM tip in UHV [39].

Bartels *et al* [9] have performed a systematic study of adsorbate lateral manipulation with an STM. The tip–adsorbate distance was used to change the type of interaction, allowing them to reach different manipulation regimes. The type of regime is detected by the recorded motion of the tip while maintaining the tunnelling current constant (constant current mode). The tip is given a linear trajectory with constant lateral speed; hence the heights of the tip are an indication of the adsorbate trajectory. This is shown in figure 1. As a consequence of their findings, Bartels *et al* [9] have classified lateral manipulations according to the following modes:

(i) The *pulling* mode where the tip–adsorbate interaction is attractive, leading to an adsorbate discontinuous tracking of the tip's linear motion.
(ii) The *sliding* mode can be made accessible by increasing the tip–adsorbate interaction. The adsorbate motion is continuous following the tip.
(iii) The *pushing* mode is attained when the adsorbate's motion is discontinuous again. Here, the tip repels the adsorbate.

Numerical simulations are essential to understand the mechanisms involved and the possible interactions between the tip, adsorbate and substrate. By comparing numerical results with the experimental measurements, it is possible to extract fundamental information such as the nature of interactions, or details such as subgroup conformation changes in large molecules. However, the main objective of manipulations is to create new, artificial, nanostructures with unconventional properties. Formally, *ab initio* methods are the best ones to use for all systems with a quantum mechanics description, but in practice, the STM junction is too large to take into account with a full *ab initio* scheme. Depending on the nature of the system, suitable theoretical methods will be chosen, mostly from semi-empirical or empirical methods; see section 2.

Most of the available simulations study the manipulation conditions such as the tip height, the potential energy surface (PES) modification, the force components in each

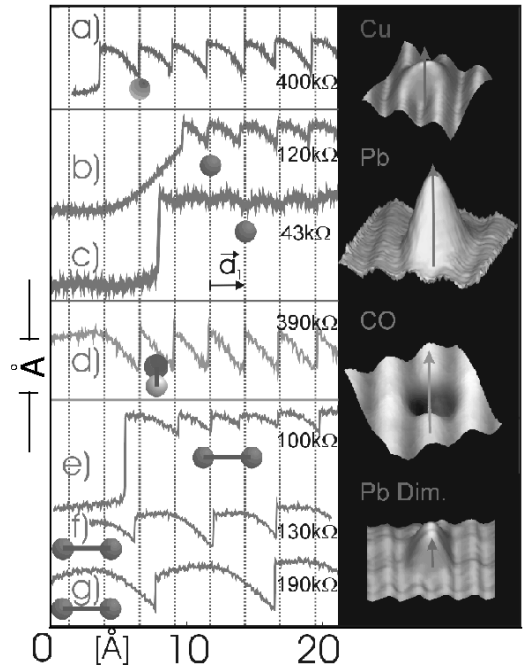

Figure 1. The left column shows unfiltered tip height curves during manipulation of an (a) Cu atom, ((b), (c)) Pb atom, (d) CO molecule, ((e)–(g)) Pb dimer [1–10]. The tip moves from left to right, and the tunnelling resistances are indicated. All the vertical dotted lines correspond to fcc sites. The initial sites of the manipulated species are indicated by small sphere models. The right column are corresponding STM images of the each adsorbate. The arrows indicate the direction of tip movement. Reprinted with permission from [9]. Copyright 1997 by the American Physical Society.

direction, the corresponding adsorbate positions and so on. There are only a few cases where tunnelling information (i.e. the tip height variation in a constant tunnelling current mode or the tunnelling current variation in the constant height mode) is calculated simultaneously with the manipulation process.

The total energy of the 'tip–adsorbate–surface' system can be decomposed as follows:

$$E_{\mathrm{tot}} = E_{\mathrm{tip}} + E_{\mathrm{ads}} + E_{\mathrm{surf}} + E_{\mathrm{tip-ads}} + E_{\mathrm{tip-surf}} + E_{\mathrm{ads-surf}}. \tag{1}$$

At each position of the tip apex (x, y, z), the total energy of the system, E_{tot}, can be minimized by classical algorithms of optimization or by molecular dynamics. In nearly all of these calculations, tip and surface are supposed to be rigid so that in certain conditions, the variation of the tip energy, E_{tip}, and of the surface energy, E_{surf}, can be assumed to be zero. Furthermore, in the case of single-atom manipulation, the variation of the internal energy of the adsorbate, E_{ads}, can also to be taken as zero. Then, for the purpose of simulation and analysis of adsorbate manipulation, the total energy reduces to the sum of the interaction energy between the tip and the adsorbate $E_{\mathrm{tip-ads}}$, the tip and surface, $E_{\mathrm{tip-surf}}$, and the adsorbate and the surface, $E_{\mathrm{ads-surf}}$.

3.1. Single-atom manipulation

3.1.1. Simulation of 'mechanical' properties of manipulation. One of the first examples of the mechanical manipulation of a single Xe atom on Cu(110) was presented by Bouju *et al* in 1993 [40]. The interaction energy, $E_{\mathrm{ads-surf}}$, of a Xe atom on the copper surface is modelled by

a repulsive short range Born–Mayer part E_s and an attractive long range component, E_d, for the van der Waals interaction. The parameters used in the Born–Mayer part are determined for the Cu(110) surface by fitting the total energy $E_{ads-surf} = E_s + E_d$ to the experimental value of the adsorption energy at low coverage. The attractive dispersion energy E_d is determined from the generalized susceptibility theory [41]. The linear susceptibility of the isolated atom used in this theory is obtained by performing a multipolar expansion of the response of the surface to an external excitation.

The STM tip position is defined as the position of the terminal atom of the tip apex. As for the Xe/surface total energy, the tip–surface interaction $E_{tip-surf}$ is also composed of a short range Born–Mayer potential and a long range part. Moreover this last part is expressed in terms of a multipolar propagator of the tip and the multipolar polarizability of the adsorbate, in order to take into account the specific arrangement of the metallic tip apex.

In this paper, three regimes of the tip–sample distance z are distinguished. For $z > 0.9$ nm, the influence of the tip on the PES, E_{tot}, is minimal. For 0.6 nm $< z <$ 0.9 nm and the tip at the hollow site where the Xe atom sits, the modification of the PES due to the tip becomes significant. However, it is only for a value of z under 0.64 nm that the Xe atom becomes more stable under the tip, trapped by some kind of van der Waals well, and follows the tip when it runs along the $[0\bar{1}1]$ direction. Finally, for $z < 0.6$ nm, the potential energy under the tip becomes higher than at the other sites on the surface and the adatom escapes from the tip.

In a paper by Buldum and Ciraci [42], both the lateral translation of Xe atom on Pt(111) and the vertical reversible transfer of Xe between two flat Pt(111) electrodes are studied. For the lateral manipulation, the Xe/surface interaction is described by the empirical potential introduced by Barker and Rettner [43] which has the 6–12 form. This potential is expressed as a sum of non-spherical, pairwise additive potentials and an additional term, which describes the interaction of Xe with the delocalized conduction electrons of the metallic surface. The interaction between Xe atom and W atoms of the tip is described by a classical Lennard-Jones pairwise potential. In this potential, the many-body effects are taken into account by scaling parameter values. During the calculation, the electrodes are taken as rigid and interatomic interactions such as Pt–Pt, Pt–W and W–W are not taken into account in the total energy calculation. The possible manipulation conditions as a function of tip height are identified by molecular dynamics calculations. As for other manipulation simulations, these conditions depend strongly on the tip–surface distance z. Due to the close-packed nature of the (111) surface, the Xe atom does not follow a straight trajectory in the surface plane. The effect of the tip becomes significant only for $z < 0.75$ nm. Upon the interaction with the tip, Xe shifts first sideways and is carried by the tip for 0.5 nm $< z <$ 0.7 nm, whereas it is pushed at smaller z. Furthermore, the particular atomic arrangement of the tip also has an important influence on the behaviour of Xe.

In 1999, Kürpick and Rahman [44] applied potentials derived from the embedded atom model (EAM) [45] to simulate Cu adatom manipulation on the Cu(111) surface with a (100) microfaceted step. For this simulation, functions fitted by Voter *et al* [46] and by Foiles *et al* [47] are used, and similar results are obtained. A tip–surface distance dependence of the manipulation processes is also observed as in the above-cited cases. This behaviour is mainly attributed to the modification of the PES by the presence of the tip apex. Although, the qualitative changes in the diffusion barriers of an adatom in the presence of a tip does not depend on the details of the tip, quantitative results are sensitive to the shape and the tip–surface separation.

More recently in a paper by Pizzagalli and Baratoff [48], manipulations of an Ag adatom on Si(001) were investigated by using a combination of a semi-empirical quantum chemistry method (ASED-MO) for short range chemical bonds and an analytical Hamaker-type method

for the long range van der Waals contributions. The ASED (atom superposition and electron delocalization) method used in this paper is based on the original work of Anderson and Hoffmann [49] in which a two-body nuclear–nuclear repulsive energy was added to the extended Hückel [50] binding energy in order to predict bond lengths and force constants in diatomic molecules. This method is also used in geometry optimization for polyatomic organic molecules [51], and for organometallic molecules by introducing a distance dependence in the Wolfsberg–Helmholz equation [52]. In this paper, four possible manipulation processes are identified. Of the four manipulation processes, three correspond to the above pulling, sliding and pushing modes when a Si(111) tip is used. If the tip is metallic (composed by Au atoms for example), only the pushing mode is achieved. The tip structure and orientation dependence are studied. In this study, the force variations in different manipulation modes are very similar to the height signatures observed in the constant current mode of STM.

3.1.2. Simulation of manipulation signals: tunnelling current and tip height variations. A tunnelling current calculation associated with the mechanics was performed just after the experimental demonstration of Bartels *et al* [9]. For the mechanical part, an approach similar to that used in [40] is employed while the corresponding tunnelling current is calculated with a scattering matrix formalism [53]. The current is connected to the dynamics of a Xe atom through the tip positions. The simulation is performed by calculating the tunnelling current in connection with the mechanics of the tip. Furthermore, to complete their investigation, the tip structure and dynamical effects are also investigated. Finally, constant height STM signals of the pulling and pushing manipulation modes are revealed while the sliding mode is not observed. These current signals are very similar to that of the recorded tip height variations (figure 1) in the constant current mode. However, a direct comparison between simulation results and experimental measurements is not possible. To overcome this drawback, a numerical virtual STM system was developed in 1999 [54]. In this virtual STM, a feedback loop signal is included directly in the complete calculation procedure. This signal is used as a direct diagnostic of the mechanics of the adsorbate during manipulation. This complete self-consistent scheme realistically reproduces a working STM, although it is computationally very demanding.

In summary, by means of simulations of mechanical properties, a detailed interpretation of the mechanisms involved in manipulation processes can be obtained. In these simulations, the numerical precision requirements are strongly linked with the theoretical method employed. The calculation of tunnelling currents can be included in the manipulation simulations by the well proved electron scattering formalism [53] or Green functions methods [55]. The association of tunnelling and mechanical calculations allows a quantitative comparison with experimental measurements.

Kühnle *et al* [56] have developed a numerical scheme for manipulations. This model does not intend to simulate manipulation mechanisms like the examples given above, but to be a simple numerical tool for experimentalists to use to determine the manipulation regime and the atomic paths. The STM junction is described as a combined potential of the tip and the surface. The generic (111) surface of an fcc metal is simulated by a superposition of three sinusoidal waves. While the tip is simulated by a Morse-type potential in which both attractive and repulsive parts are included. Of course, this simple numerical model is justified under strict conditions and assumptions. However, it provides a straightforward qualitative understanding of experimental situations with a minimal computational effort. Moreover, temperature effects can be taken into account by including a Boltzmann probability to overcome potential barriers. This work shows that the transition from the pulling mode to the sliding mode is achieved by progressively decreasing the tip height. In the same way, this method has revealed that the

periodicity of manipulation signal reflects the path followed by the adatom during the lateral manipulation process.

3.2. Single-molecule manipulation

The first single-molecule manipulation by an STM tip was achieved in 1992. There a CO molecule was manipulated on the Pt(111) surface [57]. The first complex molecule to be manipulated was the Cu-tetra[3,5-di-tert-Bulfinch]porphyrin (Cu-TBPP) molecule on Cu(100) at room temperature—by Jung *et al* in 1996 [58]. However, these first manipulations did not record the tunnelling current signals in real time. The only way to be sure that a manipulation was achieved was to check the STM image afterwards, and to compare it with the one taken before. This needs a reference on the surface such as a defect near the adsorbate. In 1997, Bartels *et al* showed detailed tip height signals during the constant current mode manipulation [9]. Furthermore, they also observed that the pulling and sliding modes are dominant in single-atom manipulations, while the pushing mode is the principal one in single-molecule manipulations. The first manipulations of Cu-TBPP and C_{60} were performed in UHV conditions and at room temperature [58, 59]. The constant current mode manipulation is used as in the case of small molecules or atoms. However, when the temperature turns to a very low value, this manipulation process is not possible. This is mainly due to the lack of a thermal bath which smooths the potential energy surface. In the constant current mode, the tip height is kept to the reference current value during a scan in a way that limits the interaction between the tip and the molecule. This weak interaction is not enough to push the adsorbate. The only possible way to manipulate the adsorbate is to increase the tip–molecule interaction. For this reason, Moresco *et al* proposed to use the constant height manipulation mode for the low temperature case [60].

The objective of the first simulations of large molecule manipulation was to explain how such a large molecule can be acted upon. In the case of the Cu-TBPP molecule [58], it was shown that the manipulation process could be divided into two major steps. The first one is the approach of the tip apex to the molecule until the point before the molecule starts moving. During this step, the molecule deforms its geometry to relax the mechanical pressure of the tip. However, when this pressure exceeds the limit at which the molecule can be deformed, the second step of the manipulation begins. The molecule starts moving (see figure 2). During this second step, the graph representing the angle between the two front molecular legs explains clearly the mechanism during the molecular translation. Similarly, in the case of the simulation of C_{60} along a monatomic step edge on Cu(100), one can understand that the C_{60} molecule slips linearly along the step edge until it hits a kink. To pass over this kink, the molecule turns around in a plane parallel to the surface, and once the kink is passed, the molecule continues gliding [61]. In a last example of Cu-TBPP molecule manipulation at low temperature [62], the tunnelling current calculation was associated with the mechanical one. By decomposing the main current into branches passing through each leg, it was possible to demonstrate that the two legs sticking to the tip apex during the translation are rigid and the current passing through these legs reflects only the periodicity of surface atoms. However for the two other legs, the current passing through them has also a periodicity reflecting that of the surface, but with more variation in a period. These variations are the consequence of the additional freedom of these two legs.

In these manipulation simulations only physisorbed molecules were considered, while for chemisorbed molecules, quantum chemistry methods are necessary to take into account charge transfer between the adsorbate and the surface. The main obstacle to using quantum chemistry methods is the size of the tip–molecule–surface system which requires big computer

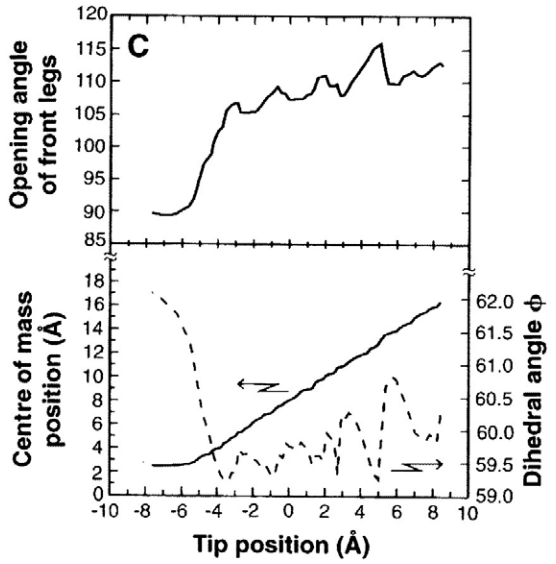

Figure 2. Lower panel: displacement of the porphyrin molecule's Cu centre atom (solid curve) and rotation (dihedral) angle ϕ of one of the front legs (dashed curve) as a function of tip displacement. The dihedral rotations of the two front legs are uncorrelated. Upper panel: opening angle between the two front legs in the plane of the molecule. The out-of-phase discontinuity of the torsion angle results in the discontinuous displacement of the molecule. Reprinted with permission from [58]. Copyright 1996 AAAS.

resources. In the case of physisorbed molecules, the molecule can be described rather precisely through classical molecular mechanics methods such as MM2 [63], while the tip–molecule and molecule–surface are roughly described by Buckingham or Lennard-Jones potentials.

4. Molecular manipulation by inelastic electron currents

Inelastic effects are perhaps the best means of inducing controlled manipulations at the atomic level. During the flow of a current through a region of atomic dimensions, there is a non-zero probability of exciting vibrations. The current furnishes the energy to do so. In other words, the electron flow does not proceed in an elastic regime any longer. There exist a wealth of techniques for controlling currents at the atomic level which allow us to induce inelastic effects and to control the dynamics of atomic size objects. The STM is one such tool. Thus, atomic manipulations can be performed by varying the set of the different parameters of the STM (current, voltage and tip–surface distance) which together with the subatomic extension of the tunnelling current make the STM a unique tool for molecular manipulation using inelastic effects [10, 11, 64–67].

Inelastic effects are particularly interesting when they are induced in a controlled manner. An example of the control attainable by the STM is the realization of vibrational spectroscopy on single molecules [10]. This technique is the STM generalization of the inelastic electron tunnelling spectroscopy (IETS) in metal–insulator–metal junctions [68, 69]. When the voltage bias matches the frequency of a vibration localized in the tunnelling gap, electrons can yield energy to excite one quantum of vibration. The inelastic electron ends up in a different conduction channel. Since the sum over final states is larger, the current increases providing a measurable signature at the voltage that matches the vibration quantum. Hence, IETS consists

in the detection of an increase of conductance at the vibration frequency [68]. The actual story is more complicated due to the many-body character of inelastic conductance [70–76]. The STM allows a dramatic spatial localization of the tunnelling current, enhancing IETS with the ability to spatially map the variations of conductance [10, 77, 78].

Recently, similar vibrational signatures in the high conductance regime have been revealed. Experimental evidence has been produced characterizing for the first time the signature of vibrational excitation of an atomic gold chain in its electrical conductance [79]. The most remarkable finding of this experiment is perhaps the revelation that at the atomic size, inelastic effects are mode selective. Indeed, at low temperature (5 K) Agraït and co-workers [79, 80] show that only few chain modes contribute to the change in conductance due to inelastic effects.

Hence there is a wealth of experimental data revealing the controlled excitation of a few quanta of vibration (in most cases only one quantum) in both the low conductance (or tunnelling) and the high conductance regimes. It is then interesting to explore and characterize quantitatively all these experiments. The calculation of inelastic currents is complicated by the fact that the electron energy is no longer a good parameter in accounting for the electronic transmission because after an inelastic transition the transmitting electron changes its energy [81]. The Landauer equation which says that the current is just the addition of the transmission probabilities for an electron at the energies spanned by the voltage bias times some universal constants needs to be revised.

Meir and Wingreen [82, 83] go beyond the Landauer formalism to the inclusion of inelastic effects in conductance calculations, but it has been very recently seen that the more involved formalism of Meir and Wingreen has started to be applied at the same level of sophistication as the simpler Landauer approach [84, 85].

In the tunnelling or low conductance regime the voltage drop takes place in the tunnelling junction. In an STM, the electrodes are the metallic tip and the substrate. These electrodes are then considered to be in equilibrium, so as to have a well defined chemical potential. There are then two chemical potentials that differ by the applied bias voltage times the electron charge. Current flows because there is a probability that the electron tunnels through the junction from an occupied state in the high chemical potential electrode to an unoccupied state in the other electrode. Tunnelling means that the electron wavefunction is exponentially decreasing with distance, as it corresponds to an electronic state at bound energies. This description of tunnelling conduction relies then on the fact that, thanks to the insulating gap (in STM it is generally ultrahigh vacuum), the electrodes are basically unperturbed, since they are in local equilibrium, and one can therefore keep a complete and accurate description in terms of the eigenstates of each electrode. The total energy calculations of section 2 are then directly applicable to the tunnelling junction.

The conduction process can be computed by using Bardeen's transfer Hamiltonian [86, 87] which is basically a perturbation approach to the influence of the tip on the substrate's wavefunctions. In the case of adsorbates this procedure is very accurate due to its performance and the accurate electronic structure calculations available nowadays; see section 2. Tersoff and Hamann [88] used the wavefunction of a spherical tip and obtained that the tunnelling conductance, σ, is proportional to the local density of states (LDOS), ρ, evaluated at the Fermi level (chemical potential of the substrate):

$$\sigma \propto \sum_{\mu} |\psi_{\mu}(\mathbf{r}_0)|^2 \delta(E_{\mathrm{F}} - \epsilon_{\mu}) = \rho(\mathbf{r}_0, \epsilon_{\mathrm{F}}). \tag{2}$$

The LDOS is a density of states ($\delta(E_{\mathrm{F}} - \epsilon_{\mu})$) weighed by the spatial information of each state contributing ($|\psi_{\mu}(\mathbf{r}_0)|^2$). This quantity is evaluated at the tip's centre of curvature ($\mathbf{r}_0$) and at the Fermi level (E_{F}). A first success of such a result is that the STM is interpreted as a probe for reading the electronic structure of the substrate at a certain distance from the surface ($\mathbf{r}_0$)

and at the substrate's Fermi level. This last result is a consequence of linear response theory which is justified in the limit of low bias voltage.

In the case of molecules adsorbed on metal surfaces, Tersoff and Hamann's approach yields a very good description of the STM constant current image when the substrate's electronic structure (eigenvalue ϵ_μ and wavefunction $\psi_\mu(\mathbf{r})$) is evaluated within DFT and with a plane wave code; see section 2.

Chen [89] has given a systematic way of improving on the description of the STM tip by using Bardeen's theory plus a description of the tip's electronic structure in terms of a spherical harmonic expansion about the centre $\mathbf{r}_0$. The first spherical harmonic recovers the Tersoff and Hamann result. Hofer and co-workers have used Bardeen's theory to treat tip and substrate within the same level of accuracy; for a review see [90].

In the calculation of elastic tunnelling currents there are a wealth of results building on Bardeen's approximation with the advantage that the non-equilibrium part of the treatment is treated perturbatively and one can make use of the accurate numerical work developed for equilibrium electronic structure calculations. Is there a way to include inelastic effects in Bardeen's treatment?

The answer is yes. The electron–vibration coupling is usually a weak interaction. Hence it can be treated perturbatively. This is easily accomplished using Green functions. Then it is interesting to have Bardeen's current calculations expressed in terms of Green functions. This has been done in [91–94]. The greatest advantage of using Green functions is that by slightly complicating the formulation, one has access to including many-body effects which turn out to be fundamental in inelastic transport. The tunnelling current can be expressed then:

$$I(V) = \frac{2e^2}{\hbar\pi}\left(\frac{\hbar^2}{2m}\right)^2 \int_{\epsilon_F}^{\epsilon_F+eV} \mathrm{d}\omega\, \mathrm{Tr}\big(\{\overleftarrow{\nabla}_1 - \overrightarrow{\nabla}_1\}\,\mathrm{Im}\, G^r_T(\mathbf{r}_1, \mathbf{r}_2, \omega) \times \{\overleftarrow{\nabla}_2 - \overrightarrow{\nabla}_2\}\,\mathrm{Im}\, G^r_S(\mathbf{r}_2, \mathbf{r}_1, \omega)\big). \tag{3}$$

This equation should be interpreted in the following way. The current depends on the voltage through the limits of the integration over the Green functions energies ω. The Green functions are retarded ones. The trace, Tr, includes a surface integration over a fictitious surface in the region of no interaction between tip (T) and sample (S), and we calculate the flux of the nabla operators through this surface [93]. This is the extension to Green functions of Bardeen's approach where the flux of nabla operators acting on the two-electrode wavefunctions is calculated over the fictitious surface. The nabla operators act on the coordinate that their subindex denotes and onto the Green function that the arrow points at. If there is no Green function, we make use of the cyclic property of the trace, and rotate the nabla and Green function so there is no ambiguity about where the nabla operators act. From now on atomic units will be used unless otherwise stated ($\hbar = m_e = e = 1$).

The substitution of single-particle Green functions (and in equilibrium) leads naturally to the customary Bardeen formula [93]. These Green functions are for the tip

$$G^{a\,(r)}_T(\mathbf{r}, \mathbf{r}', \omega) = \sum_m \frac{\psi_m(\mathbf{r})\psi^*_m(\mathbf{r}')}{\omega - \epsilon_m - (+)\mathrm{i}\delta} \tag{4}$$

where the a (r) superscript refers to advanced or retarded Green function, given by an imaginary infinitesimal $-$ ($+$)δ respectively. For the tip's single-electron wavefunctions we are using Latin subindices: $\psi_m(\mathbf{r})$. The Green functions for the sample are

$$G^{a\,(r)}_S(\mathbf{r}, \mathbf{r}', \omega) = \sum_\lambda \frac{\psi_\lambda(\mathbf{r})\psi^*_\lambda(\mathbf{r}')}{\omega - \epsilon_\lambda - (+)\mathrm{i}\delta}. \tag{5}$$

Now one can introduce the electron–vibration coupling in equation (3) by using many-body Green functions. These functions can be evaluated with Dyson's equation. Even in the

case where a local vibration is assumed, and when the one-electron structure is well known, Dyson's equation cannot be solved and some further approximations are mandatory; see for example [75]. The theory becomes numerically computable with a small effort when just the first term in the Born series of the Green function is retained. Galperin *et al* [75] call this approximation the lowest order perturbation theory (LOPT).

As we stated in section 2, the problem is enhanced by considering the coupled electronic and nuclear degrees of freedom. In the present formulation of Green functions this translates into the need of including a coupled set of Dyson's equations for both the electron and the vibration. The problem is totally tractable when only one quantum of a localized vibration is considered. In this case the vibration Dyson's equation is analytically solvable and closed expressions for numerical computation can be developed. In the context of Bardeen's approximation this has been thoroughly expounded in [74].

In the following two subsections we will review some results about the simulation of inelastic effects in currents. The first subsection will address the evaluation of vibrational spectra as revealed by IETS-STM. In the second subsection, we will extend the theory to treat reactions induced by the excitation of a particular mode, giving rise to mode-selective chemistry.

4.1. Vibrational spectroscopy using tunnelling electrons

The coupled set of electronic and nuclear coordinates renders the tasks of evaluating nuclear evolution under inelastic effects very complex. Besides having to make the approximations needed to evaluate the tunnelling current, we are thus forced to simplify the nuclear terms. In the case when only one quantum is excited, one can perform three simplifying approximations:

(i) linearize the electron–vibration coupling in the nuclear coordinates,
(ii) use harmonic oscillator wavefunctions for the nuclear coordinates,
(iii) assume fast damping rates.

The first approximation gives us the small parameter of the expansion: the mode displacement δQ_i, because it is always evaluated for the mode ground state or a low energy state. Both are very localized. Let us consider the normal vector $\vec{Q}_i$ of the mode i. Then the Hamiltonian can be expanded in a Taylor series on the normal vectors:

$$H = H_0 + \sum_i \frac{\partial H}{\partial \vec{Q}_i} \cdot \delta \vec{Q}_i + \frac{1}{2} \sum_{i,j} \delta \vec{Q}_i \cdot \frac{\partial^2 H}{\partial \vec{Q}_i \partial \vec{Q}_j} \cdot \delta \vec{Q}_j + \cdots \tag{6}$$

and the perturbing potential, δH, is taken as

$$\delta H = H - H_0 \approx \sum_i \frac{\partial H}{\partial \vec{Q}_i} \cdot \delta \vec{Q}_i.$$

The second approximation yields analytical transition matrix elements connecting different excited oscillator states. This is very convenient because the nuclear coordinates are easily factored out of the problem. Hence an electronic transition from state $|\nu\rangle$ to state $|\mu\rangle$ while exciting the vibrator, $|0\rangle \leftrightarrow |1\rangle$, once is given by

$$\langle 0, \nu|\delta H|1, \mu\rangle \approx \sum_i \langle \nu|\frac{\partial H}{\partial \vec{Q}_i}|\mu\rangle \cdot \langle 0|\delta \vec{Q}_i|1\rangle, \tag{7}$$

where the matrix element $\langle 0|\delta \vec{Q}_i|1\rangle$ is analytical and is given by

$$\langle 0|\delta \vec{Q}_{i,p}|1\rangle = \sqrt{\frac{\hbar}{2m_p\omega_i}}\vec{\epsilon}_{i,p}. \tag{8}$$

Here $\vec{\epsilon}_i$ is the unitary displacement vector on the coordinates of the different nuclei p, of mass m_p, when the mode i, of frequency ω_i, is excited (hence $\vec{\epsilon}_i = (\vec{\epsilon}_{i,1}, \ldots, \vec{\epsilon}_{i,p}, \ldots, \vec{\epsilon}_{i,N})$ for N-nuclei). More details can be found in [74, 76].

The third approximation takes care of the vibration Green function by imposing an average occupation of zero quanta in the vibrator. This assumption is generally true in the obtaining of IETS with an STM because of the efficient damping of molecular modes in contact with a metal surface; see for example [95] and references therein. Typical damping rates are a factor 10 to 100 faster than the tunnelling electrons: the time between inelastic processes is orders of magnitude longer than the de-excitation time of the molecular mode. Hence, we can safely conclude that the molecule is de-excited between inelastic processes. This assumption has been proven to be wrong in the case of vibrational excitation in the high conductance regime, such as for vibrational excitation of monatomic gold chains [85], and the mean occupation of the excited chain mode is different from zero during the excitation process.

The actual inelastic contribution to the conductance, σ, is quite involved to calculate. References [74, 76] give a detailed account of the obtaining of the final equations in Bardeen's approximation, equation (3), and their Tersoff–Hamann equivalent. In [73, 95] the many-body extension of Tersoff–Hamann theory to the treatment of IETS-STM is presented. Briefly, the inelastic contribution to the change in conductance, $\Delta\sigma$, will be caused by the change in the LDOS due to the vibration. Now, the problem is complicated by the many-body aspects of the theory. There is a first term that can be traced back to a transfer of a quantum of vibration by the impinging electron. This is called the inelastic contribution to the change in conductance [74, 76]. The relative change in differential conductance, η_{ine}, is then given by

$$\eta_{\mathrm{ine}}(\mathbf{r}_0) = \frac{\Delta\sigma}{\sigma}. \tag{9}$$

To leading order in electron–vibration coupling and using equation (2) this term is given by

$$\eta_{\mathrm{ine}}(\mathbf{r}_0) = \frac{1}{\rho(\mathbf{r}_0, \epsilon_{\mathrm{F}})} \sum_{\mu} \left| \sum_{\lambda} \frac{\langle \psi_\lambda | \delta H | \psi_\mu \rangle \psi_\lambda(\mathbf{r}_0)}{\epsilon_\mu - \epsilon_\lambda + \mathrm{i}0^+} \right|^2 \delta(\epsilon_{\mathrm{F}} - \epsilon_\mu). \tag{10}$$

Here we have taken the quasistatic limit, $\hbar\omega_i \to 0$. $|\psi_\lambda\rangle$ are the unperturbed one-electron states appearing naturally in the LOPT, and ϵ_λ the corresponding eigenenergies. The perturbing potential, δH, is obtained above, equation (6). For a detailed account of the numerical implementation of these equations, please read references [74, 76, 95].

This equation says that there is an increase of conductance due to the modulation of the wavefunction by the vibration, because the squared term is just the square of the perturbed electronic wavefunction. The spatial resolution of the wavefunction carries the information of the exponential decay in vacuum of the tunnelling probability. Hence, during the vibration this tunnelling probability will be modulated, in a way given by the change of the wavefunction.

The second contribution to the change in conductance at the same order in the electron–vibration coupling has been termed the elastic contribution. The name originates from the fact that the initial and final electron states are at the same energy; they do not differ in a quantum of vibration. The physical origin of this term is the many-body character of electron transport in the presence of vibrations. In the absence of vibrations one can approximate the many-body wavefunctions in terms of one-electron wavefunctions, that are solutions of an effective one-body Hamiltonian. When the electron–vibration coupling is included the one-electron wavefunctions are no longer eigenstates of the Hamiltonian. The vibration mixes them up. The complexity appears because the full wavefunction is antisymmetric under electron exchange, i.e. two electrons cannot be in the same quantum state. The elastic contribution reflects the exchange of two electrons mediated by the electron–vibration interaction. This exchange term

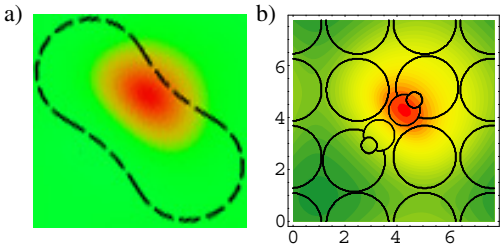

Figure 3. Spatial distribution of the change in conductance over a singly deuterated acetylene molecule chemisorbed on a Cu(100) under an STM tip. The bias voltage is at 266 meV [10] and the second derivative of the current with respect to the voltage is recorded as a function of the tip location. (a) Experimental data from [10]. The dashed curve is a contour of the constant current image of the $C_2HD/Cu(100)$ system. (b) Theoretical results from [73]. The agreement between experiment and theory is quantitative. The theoretical inelastic image shows the localization of the change in conductance about the vibrating D atom.

gives a negative contribution to the change in conductance due to the antisymmetric character of the many-body wavefunction under exchange of two electrons. This elastic contribution is given by

$$\eta_{\mathrm{ela}}(\mathbf{r}_0) = \frac{-2\pi^2}{\rho(\mathbf{r}_0, \epsilon_{\mathrm{F}})} \sum_{\mu} \left| \sum_{\lambda} \langle \psi_\lambda | \delta H | \psi_\mu \rangle \psi_\lambda(\mathbf{r}_0) \delta(\epsilon_\mu - \epsilon_\lambda) \right|^2 \delta(\epsilon_{\mathrm{F}} - \epsilon_\mu). \tag{11}$$

The notation is the same as in equation (10). There are two fundamental differences between equations (10) and (11). The first one is the sign: the elastic contribution, equation (11), is negative. It is the term responsible for the decrease in conductance as we announced. The second difference is the range of evaluation of the inner summation over electronic states: in equation (11) this summation is restricted to states at the Fermi level, while in equation (10) it extends over all energies. Hence, the elastic contribution, equation (11), will become particularly important when the density of states is very high at the Fermi level: namely, in the case of a sharp resonance at the Fermi level.

The quality of the results obtained with the simple LOPT summarized above is good. The results obtained are in good agreement with the experimental data and have allowed us to discuss and analyse the molecular modes excited with the STM. Indeed in the case of acetylene C–H stretch excitation the agreement is both in absolute magnitude and in geometrical dependence of the inelastic signal, giving confidence in the assignment of the excited molecular modes predicted by the theory; see figure 3 and references [73, 96]. In the case of the frustrated rotation of CO [95], the agreement is within a factor 2 of the results obtained by Lauhon and Ho [97], but closer to the results of Heinrich *et al* [98]. The reasons for the success of the above calculations lie in the accurate evaluation of the electron structure in combination with realistic electron–vibration couplings, respecting the symmetry and strength of modes and matrix elements. Other issues originating from the above three approximations plus the absence of tip structure are probably less relevant provided that the substrate electron–vibration structure be calculated with enough precision.

Recently, Galperin *et al* [75] concluded that the LOPT is generally accurate enough in the evaluation of inelastic transitions, except perhaps for the actual lineshape (bias voltage dependence) of the change in conductance, where they claim that a more elaborate treatment is needed.

In [74] an analysis on the change of conductance in terms of the molecular mode symmetry and the electronic structure at the Fermi level is performed by inspecting three different chemisorbed systems, $C_2H_2/Cu(100)$, $O_2/Ag(110)$ and $NH_3/Cu(100)$.

4.2. Single-molecule vibrational chemistry

Inelastic electron tunnelling spectroscopy is a non-destructive probe because the adsorbate molecule is rarely excited beyond one quantum. In order to induce molecular reactions certain barriers need to be overcome. This needs highly vibrationally excited molecules. Hence, the regime of inelastic excitation changes in order to efficiently excite the molecule.

Nevertheless, recent results [11] show that one can overcome certain molecular barriers in the limit of one quantum excitation. This has an especial interest because it allows an enhanced control over the reaction and in particular one can choose the reaction pathway. However, energy injection in chemisorbed molecules on metals is usually very difficult because vibrational relaxation is extremely fast. At low temperatures ($T \approx 5$ K), this is mainly due to the electron–hole pair continuum that efficiently dissipates the energy localized in the molecule. Therefore, different processes must be used in order to pump enough energy into the molecule before it is dissipated.

Simulations of these processes become increasingly difficult as the electronic and nuclear degrees of freedom have to be treated with accuracy and in realistic situations. We have seen that electronic states and vibrational transitions can be quite accurately accounted for as in the case of IETS-STM. There, the advantage was to integrate analytically the nuclear motion. Under reactions or important nuclear evolutions these approximations are not available any longer. Hence explicit numerical nuclear dynamics needs to be taken into account.

In the recent literature there are two basic approaches to the problem of reactions induced by the STM. The first one relies on approximations akin to the one effected above for IETS: truncation of harmonic potential wells, in order to estimate easily and quickly the effect of increasing vibrational excitations [99–103]. This approach has many inconveniences. In particular, it neglects intermode coupling due to anharmonicities which has been proven to be fundamental in nuclear evolution after vibrational excitation [3, 11, 104, 105]. It is far from quantitative, and it incurs the problem of how to split a complex transition into different meaningful physical processes. However, it has the advantage of providing a means of analysis, assigning characteristic times to the possible different processes. In this way, Salam *et al* [103] have provided some simple rules that differentiate between systems undergoing a single-electron excitation (desorption induced by electron transitions, DIET like) or multiple electron excitations (desorption induced by multiple electron transitions, DIMET like).

The second approach performs the *correct* nuclear dynamics while trying to have the best estimates for the actual potential that directs the evolution. This is a tremendous task and the potentials used range from fits to the experimental data, to more or less computed ones. On top of the treatment of the nuclear evolution, the electronic event is either assumed to take place instantaneously, and hence the description of the electronic excitation problem is absent, or treated within a single-molecular orbital model. This last model is that of a resonance in contact with the substrate's electronic structure where the only electron–vibration coupling is introduced by means of an effective resonance lifetime [4, 106, 107]. Nevertheless, these simulations give information about processes that are absent or cannot be described in the first type of approximation. There are two excellent recent reviews [4, 108] and there have been interesting results obtained on STM induced desorption from semiconducting surfaces [109, 110].

4.2.1. Modellization of NH_3 selective translation and desorption. In this subsection we briefly review the modellization leading to the explanation of the controlled translation and desorption of ammonia molecules on Cu(100) [11]. The main theoretical results have been published in [74, 104].

Table 1. Modes involving the N–H bond in NH_3/Cu(100). The first column depicts the inelastic fraction; this fraction times the tunnelling current gives the probability of the mode excitation. The second entry is the damping rate in electron–hole pairs, expressed in s^{-1}. The third entry gives the decay rate into electron–hole pairs plus excitation of the first state of the umbrella mode. The fourth entry is the decay rate into electron–hole pairs plus the excitation of the first state of the frustrated translation mode. The last entry gives the sum over vibrational states in the translation coordinate above the translational threshold (at 30 excited states or 301 meV).

Mode: ω (meV)	η (%)	$1/\tau$ (s^{-1})	$1/\tau_{\nu U}$ (s^{-1})	$1/\tau_{\nu T}$ (s^{-1})	$\sum_{T>30} 1/\tau_{\nu T}$ (s^{-1})
ν_a: 422	0.08	0.13×10^{12}		0.33×10^{10}	0.8×10^{6}
ν_s: 408	0.08	0.26×10^{12}	0.85×10^{9}	0.25×10^{10}	0.7×10^{6}
δ_a: 200	0.02	0.09×10^{12}			
δ_s or U: 139	0.4	0.04×10^{12}			

By placing an STM tip atop an ammonia molecule [11], translation of the molecule along the surface can be effected when the tip–sample bias voltage is at 420 mV over a large current range, from some hundreds of nA to some tens of nA. At 320 mV, only desorption is attained at any possible current. At 420 mV, desorption becomes possible if the current is increased over 1 nA. Hence, by choosing the region of bias voltage and current, one can choose between desorption or translation of the molecule. Moreover, the bias voltage at which inducing the translation becomes probable coincides with the theoretical threshold for the N–H stretch mode on Cu(100). The desorption probability increases dramatically when the bias is above two quanta of the NH_3 umbrella mode. There is a clear vibrational signature in the manipulation process.

In order to gain some insight into the dynamics of NH_3 after electron injection, it is interesting to evaluate the probability of excitation of the molecular modes and their lifetimes. In particular, the coupling to different modes can be crucial to understanding the process of manipulation of NH_3 by the STM. The two evolutions of interest are the translation of the molecule and its desorption.

In section 4.1, we have seen how to calculate the inelastic electron fraction η_{ine} which is a function of the STM tip location. Here, we extend the theory to include de-excitation of molecular modes and intermode coupling. The damping of molecular vibrational modes by decaying into surface phonons is important when the molecular frequencies overlap with the surface phonon band [100]. Typically the Cu surface phonon band is below $\sim$30 meV. Hence, for most of the modes of NH_3, decay into surface phonons will be negligible (see table 1 for the relevant frequencies).

The dominant contribution to the higher energy mode damping is electron–hole excitation [111]. The rate of vibration decay into electron–hole pairs can be calculated using Fermi's golden rule, where the electron–vibration coupling described in the previous section is used. This approach has been used in [95, 112].

The decay of a given molecular vibration into a group of other molecular vibrations is greatly enhanced in the presence of electron–hole pairs. The excitation of electron–hole pairs guarantees energy conservation in the full process and reduces the number of lower energy quanta needed to match the energy of the decaying high energy mode. The calculation of the damping rate into different low energy vibrations assisted by electron–hole pairs can be carried on in a way similar to the calculation of mode damping into electron–hole pairs.

The perturbation $\delta H = H - H_0$ from equation (6) can be used in Fermi's golden rule to calculate various transition rates. Hence the leading term in a single-mode transition, i.e. the damping of the mode i of frequency ω_i from the first excited level into the ground state by

electron–hole pair excitation, is given by the first term:

$$\frac{1}{\tau} = \frac{2\pi}{\hbar} \sum_{\lambda,\mu} f_\lambda (1 - f_\mu) \left| \langle 1, \lambda | \frac{\partial H}{\partial Q_i} \delta Q_i | 0, \mu \rangle \right|^2 \delta(\epsilon_\lambda - \epsilon_\mu + \hbar\omega_i) \tag{12}$$

where f_λ is the Fermi occupation factor for the electronic state λ. Hence $f_\lambda(1 - f_\mu)$ explicitly shows the excitation of an electron–hole pair in the transition; both λ and μ are electronic states. The rate of decay of each mode into electron–hole pairs is given in the third column of table 1, expressed in s^{-1}.

Contribution (13) is identically zero when two modes are coupled via electron–hole pairs. Then, the first contribution to the intermode coupling is given by the last term in the expansion, equation (6). The probability of de-exciting one mode i from its first excited level to its ground state while exciting another mode j from its ground state to a level n of the j mode in the presence of electron–hole pair excitation is then

$$\frac{1}{\tau} = \frac{2\pi}{\hbar} \sum_{\lambda,\mu} f_\lambda (1 - f_\mu) \left| \langle 1, 0, \lambda | \frac{\partial^2 H}{\partial Q_i \partial Q_j} \delta Q_i \delta Q_j | 0, n, \mu \rangle \right|^2 \times \delta(\epsilon_\lambda - \epsilon_\mu + \hbar\omega_i - \hbar\omega_j(n)). \tag{13}$$

In this last expression, we take into account that the excitation of n quanta of the j mode will be an anharmonic process, and hence the transferred energy may not be simply proportional to the mode frequency ω_j, but a function of n, given by $\hbar\omega_j(n) - \hbar\omega_i$. The anharmonic coupling becomes readily apparent if we simplify the matrix element in equation (13):

$$\langle 1, 0, \lambda | \frac{\partial^2 H}{\partial Q_i \partial Q_j} \delta Q_i \delta Q_j | 0, n, \mu \rangle = \langle \lambda | \frac{\partial^2 H}{\partial Q_i \partial Q_j} | \mu \rangle \langle 1 | \delta Q_i | 0 \rangle \langle 0 | \delta Q_j | n \rangle. \tag{14}$$

In the harmonic approximation only $n = 1$ is different from zero. It is then the anharmonicity that allows the coupling. The second-order derivative of the Hamiltonian does not pose any particular problem and can be evaluated in the same way as the first derivative because intermode coupling implies that i and j are different modes, and effectively, equation (14) is a first-order derivative in Q_i and a first-order one in Q_j. It is then evaluated using finite differences as in [95]. When needed, the anharmonic terms have been calculated with a 1D approximation in the potential energy surface, PES, calculated for the relevant reaction coordinate.

The anharmonicity exploited here comes from the deviation of the actual PES from harmonic potential wells. This is clearly a strong source of anharmonicity when looking at the reaction path on a PES. This kind of anharmonicity is not related to the direct coupling between modes because of their own deviation from harmonic modes. In this last case, the modes are already coupled without the need for the processes described above.

The reaction coordinate for the translation mode is the displacement of the molecule's centre of mass along the [011] or the [0$\bar{1}$1] directions as can be seen in the PES; figure 4. The frustrated translation normal mode coordinates show that this is indeed the case: its amplitude $\langle 0 | \delta Q_T | 1 \rangle$ is basically a rigid 0.1 Å displacement for each atom. According to the calculations, at the experimental bias (420 mV) between tip and substrate [11, 76, 104], the symmetric stretch N–H can be excited. The N–H stretch can decay into electron–hole pairs while exciting one quantum of the frustrated translation mode. This quantity is the fourth entry of table 1. As expected, we find that the leading term in the decay is simply the damping into electron–hole pairs without other vibration excitation. The excitation of higher states of the frustrated translation mode can be calculated by evaluating numerically the matrix element $\langle 0 | \delta Q_T | n \rangle$. In our procedure, if $n = 1$, the matrix element is correctly calculated for the full vector δQ_T in the harmonic approximation. In order to take into account anharmonicities,

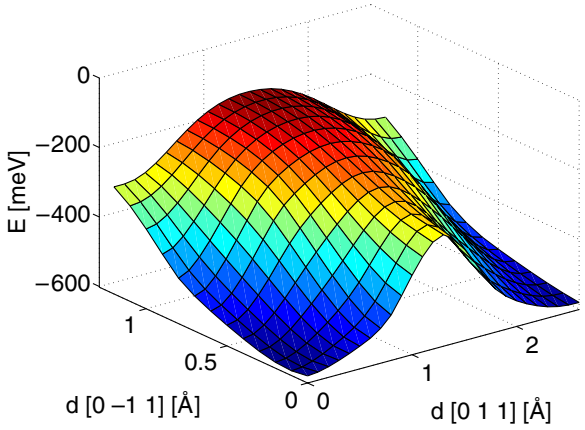

Figure 4. Potential energy surface of NH_3 along the Cu(100) surface calculated with the generalized gradient approximation using plane waves, and a 3×3 supercell where there is an ammonia molecule every three Cu atoms in the x and y directions of the surface. The plane axes are in Å, and the perpendicular axis in meV. The bridge side is at 1.29 Å along the [011] direction. It is a saddle point of 301 meV of height. The hollow site of coordinates (1.29, 1.29) Å is a maximum. The barrier from top to hollow is 456 meV. The molecule needs less energy to go from top to top through the bridge site.

we solve Schrödinger's equation in 1D for the PES of the centre of mass, and we evaluate equation (13) by multiplying times

$$\frac{\langle 0|X|n\rangle}{\langle 0|\delta Q_{\mathrm{T}}|1\rangle}$$

where X is centred on the initial position of the molecule such that $X \approx \delta Q_{\mathrm{T}}$. This factor accounts for the actual anharmonic $|n\rangle$ states of the true 1D well, because equation (14) is expressed in terms of the single quantum excitation since the finite difference method allows an accurate evaluation of the harmonic matrix elements [95]. Then, we obtain for the stretch (ν) to translation (T) coupling

$$\langle 1,0,\lambda|\frac{\partial^2 H}{\partial Q_\nu \partial Q_{\mathrm{T}}}\delta Q_\nu \delta Q_{\mathrm{T}}|0,n,\mu\rangle = \langle 1,0,\lambda|\frac{\partial^2 H}{\partial Q_\nu \partial Q_{\mathrm{T}}}\delta Q_\nu \delta Q_{\mathrm{T}}|0,1,\mu\rangle \frac{\langle 0|X|n\rangle}{\langle 0|\delta Q_{\mathrm{T}}|1\rangle}. \qquad (15)$$

Figure 5 shows the behaviour of the decay rate with the energy of the final frustrated translation mode. The decay rate plunges quickly with increasing energy of the final state. Above 300 meV the molecule can translate classically into other sites. The classical threshold is attained at the $n = 30$ state of the anharmonic frustrated translation mode. The change in wavefunction over this threshold leads to an extra kink in the decay rate function; figure 5. The rate for de-exciting the N–H stretch into a state delocalized in the translational coordinate is then given by the sum of all decay rates above $n = 30$. This is given in the fifth column of table 1.

The results presented here can be used in a master equation approach akin to the first type of approximation described earlier in section 4.2. Yet, this approach has the problems discussed above and is at best qualitative. Once the steady state is reached, i.e. no evolution of the intermediate products takes place any longer, it is easy to find the populations of the different vibrational states. Thus one can easily estimate the amount of translated molecules over the molecules in their ground state, by using the branching ratio γ_{exc}:

$$\gamma_{\mathrm{exc}} \approx \frac{1/\tau_{\nu T}}{1/\tau_\nu}, \qquad (16)$$

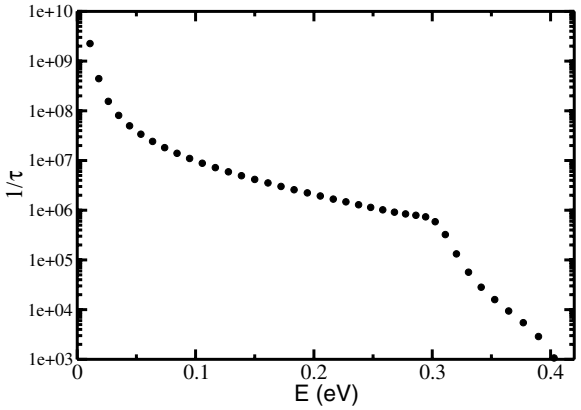

Figure 5. Rate of decay of the N–H stretch mode into excited states of the 1D PES along the [011] direction in s^{-1} versus the excited state energy in eV. Each dot corresponds to the energy of the final translational state. Above 301 meV the translational states become unbounded. The coupling matrix element decays faster with energy above the 301 meV threshold because of the extended nuclear wavefunctions.

where $1/\tau_{\nu T}$ is the rate of decay into molecules that can translate; fifth column of table 1. The total decay rate of the stretch mode has been substituted by its leading contribution $1/\tau_{\nu}$, the rate of decay into electron–hole pairs. Our calculated γ_{exc} is then an upper limit to the actual ratio of branching into the excitation of the translation.

Now, not all molecules that can translate will do it. It is here that a proper dynamical calculation, as in [108, 113], can give a quantitative estimate of the translated molecules.

The desorption process is more complicate. The desorption coordinate is given by the displacement of the centre of mass perpendicular to the surface. In order to estimate the importance of the de-excitation of the stretch molecule into desorption we have evaluated:

(i) The rate of decay of the stretch mode into the umbrella mode plus electron–hole excitation.
(ii) The correction to the decay rate given by the anharmonicity in the desorption coordinate.

The PES in the desorption coordinate has been taken from [108] and fitted to reproduce our ν_{M} mode. Hence the factor included in the matrix element of the decay rate, equation (15), is now

$$\frac{\langle 0|Z|n\rangle}{\langle 0|\delta Q_{\mathrm{U}}|1\rangle}$$

where Q_{U} is the normal coordinate of the umbrella mode and n is an excited state of the anharmonic ν_{M} mode. The barrier for desorption is 600 meV. Hence a single quantum of the N–H stretch mode is not enough. In order to estimate the possible de-excitation rates leading to desorption we use two N–H stretch de-excitations in a ladder fashion, taking into account that in the harmonic approximation $\langle 1|\delta Q_{\mathrm{s}}|2\rangle = \sqrt{2}\langle 0|\delta Q_{\mathrm{s}}|1\rangle$. The evaluation of the molecular population in the desorption limit entails the calculation of transition rates between different modes in different populations being allowed by energy conservation. Hence, we need to sum over all possible transitions in order to find the final transition rates.

In order to give a simple estimate of the importance of the stretch–umbrella coupling, we give in table 1 the rate of transition between a stretch mode and an umbrella mode while emitting electron–hole pairs. We find that the rate of de-excitation into the umbrella mode is less than the rate of de-excitation into the frustrated translation. This is due to the actual

coupling, $\partial^2 H/\partial Q_i \partial Q_j$, through the electron–hole pairs, and is not an effect of the larger phase space for smaller frequency modes. The emerging image is that of a transient excited state, where the umbrella and the stretch modes are excited simultaneously. The decay of the excited stretch into, again, the umbrella mode or simply the centre of mass mode leads to the desorption of the molecule. This reaction path is especially efficient for two reasons:

- The umbrella mode is relatively long lived.
- Only five umbrella quanta are needed to desorb.

The first fact leads to a transient state that can de-excite the stretch mode first while further exciting the umbrella mode. The second fact rules out other intermediate coupling that would need many more quanta, and hence an unlike coupling between the ground state and the desorbing state.

Studies of ammonia vibrational excitation on surfaces [108] and of photodesorption [113] show that the actual PES leading to desorption is very complicated. The umbrella mode becomes coupled with the centre of mass stretch mode (ν_M), and not even a 2D PES gives quantitative results. Hence the actual simulation of ammonia desorption from metal surfaces is far from being achieved. At most, one can currently show qualitative trends and understand the main physical effects after STM manipulations.

Nevertheless, the calculations performed so far permit one to understand the main ingredients that a molecular system needs to have to be subjectable to vibrational selective manipulations. Initially, well separated vibrational modes are needed. This is indeed the case in the ammonia system where the stretch N–H modes lie $\sim$100 meV above the next mode following in vibrational frequency (the N–H bending modes). This is necessary in order to have clear thresholds for selection by the tip's bias voltage. The electronic structure calculations have shown that $NH_3/Cu(100)$ is a weakly coupled system. The consequence is that electron–hole damping is less efficient than in strongly chemisorbed systems, and hence the damping rates are smaller with an important effect in the desorption of molecules arising by sequentially pumping a vibrational mode along the desorption coordinate (in the case of ammonia molecules, this is the umbrella mode). Finally, the role of the substrate is shown to be fundamental. It allows transitions by permitting energy conservation through the electron–hole continuum (hence the difficulty of effecting the above manipulation in semiconducting or insulating surfaces), and by enhancing the anharmonicity of molecular modes.

5. Outlook

The promise of manipulation of matter at its simplest building blocks is stirring a lot of effort in the field of adsorbate manipulations. However, the interface with the macroscopic world is necessarily complex, hampering much of the initially anticipated benefits of this field. In order to achieve an efficient nanoscale to macroscale interface many basic ingredients must be known first. Here, we give some details on what we believe must be addressed in future research. Some of these items may take a long time to develop depending on the evolution of the related fields of molecular dynamics simulations, electronic structure calculations and total energy simulations.

(i) Ground state calculations of large atomic systems (in the range of a few hundreds of atoms) are very accurate thanks to the development of DFT calculations. These calculations permit one to predict atomic dynamics with precise implications. The excitation of vibrations is a particular case, since single-quantum excitations are precisely given by ground state calculations. However, the first limitations appear here. The realistic

calculation of excited vibrators becomes very difficult and needs the development of accurate dynamics in the direction of the simulations described in [4, 107, 108].

(ii) Electronic excited state calculations are needed beyond ground state calculations. We have shown above that the heuristic use of electronic transitions between Kohn–Sham states leads to good agreement with experiments, yet the simulations of manipulations using electronically excited states will require the development of codes and calculations developed for excited states. This field is progressing rapidly with the different developments undertaken in time-dependent DFT schemes [114] as well as the GW approximation [115].

(iii) Temperature effects will receive increasing attention from the theoretical point of view. In particular, the decay mechanism on semiconductor and insulator surfaces is given by phonon excitation which depends on the phonon population and hence on the temperature [8, 65, 109].

(iv) Vibrationally enhanced molecular reactivity: NH_3 manipulation with the STM [11] has been shown to be an example of mode selective chemistry in the sense that a given pathway has been chosen by exciting a specific vibration of the molecule. This opens the possibility of inducing reactions in more complex molecules by locally exciting certain vibrations. It will be of great interest to understand whether one can actually change the reactivity or induce internal reactions of certain molecules by inducing local vibrations. In order to do this, there is a need of understanding vibrational excitation of complex molecules, and how the energy is redistributed among the different degrees of freedom. The NH_3 manipulation shows that this kind of strategy can give access to pathways that are, if not unavailable, at least populated in a very different way in conventional thermal reactions [104].

(v) Non-local interactions triggered by local effects. If one can induce chain reactions in self-assembled systems, the door to large scale manipulations from a bottom-up perspective will be open. Recent results [116] have shown that one can induce ordering and reactions of many molecules at once by acting with an STM on a semiconductor surface. It is probably the moment to investigate how inelastic electron manipulation can actually be used in collective manipulations.

(vi) Beyond the tunnelling regime, inelastic effects promise to be an active field of research in molecular electronics. The behaviour of molecule-based devices will depend on the control over the excitation of molecular vibrations that is attained. Recent theoretical results show that currents in atomic size devices do indeed efficiently populate some of the vibrational modes, but that there is a mode selectivity given by the mode symmetry and the particular electronic structure of the molecular device [79, 84, 85, 117, 118].

Acknowledgments

It is a pleasure to thank for fruitful discussions J I Pascual and E Hernández. NL and HT gratefully acknowledge financial support from ACI *Jeunes Chercheurs*. RR acknowledges the financial support of the Generalitat de Catalunya through a NANOTEC fellowship. The calculations were performed at the Centre d'Informatique National de l'Enseignement Supérieur (CINES) and the Centre de Calcul Midi-Pyrénées (CALMIP).

References

[1] Binnig G, Rohrer H, Gerber C and Weibel E 1982 *Phys. Rev. Lett.* **49** 57
[2] Eigler D M and Schweizer E K 1990 *Nature* **344** 524
[3] Ueba H 2004 *Surf. Rev. Lett.* **5** 771

[4] Seideman T 2003 *J. Phys.: Condens. Matter* **15** R521
[5] Ho W 2002 *J. Chem. Phys.* **117** 11033
[6] Stroscio J A and Eigler D M 1991 *Science* **254** 1319
[7] Tsong T T and Chang C S 1995 *Japan. J. Appl. Phys.* 1 **34** 3309
[8] Dujardin G, Mayne A, Robert O, Rose F, Joachim C and Tang H 1998 *Phys. Rev. Lett.* **80** 3085
[9] Bartels L, Meyer G and Rieder K H 1997 *Phys. Rev. Lett.* **79** 697
[10] Stipe B C, Rezaei M A and Ho W 1998 *Science* **280** 1732
Stipe B C, Rezaei M A and Ho W 1999 *Phys. Rev. Lett.* **82** 1724
[11] Pascual J I, Lorente N, Song Z, Conrad H and Rust H P 2003 *Nature* **423** 525
[12] Messiah A 1961 *Quantum Mechanics* (Amsterdam: North-Holland)
[13] Szabo A and Ostlund N S 1989 *Modern Quantum Chemistry: Introduction to Advanced Electronic Structure Theory* (New York: McGraw-Hill)
[14] Hohenberg P and Kohn W 1964 *Phys. Rev.* **136** B864
[15] Kohn W and Sham L J 1965 *Phys. Rev.* **140** A1133
[16] Kohn W 1988 *Rev. Mod. Phys.* **71** 1253
[17] Ceperley D M and Alder B J 1980 *Phys. Rev. Lett.* **45** 566
Perdew J P and Zunger A 1981 *Phys. Rev.* B **23** 5048
[18] Perdew J P, Burke K and Ernzerhof M 1996 *Phys. Rev. Lett.* **77** 3865
[19] see http://cms.mpi.univie.ac.at/vasp/
[20] Hammer B, Hansen L B and Nørskov J K 1999 *Phys. Rev.* B **59** 7413
see also http://www.fysik.dtu.dk/campos/Dacapo/
[21] Segall M D, Lindan P J D, Probert M J, Pickard C J, Hasnip P J, Clark S J and Payne M C 2002 *J. Phys.: Condens. Matter* **14** 2717
[22] see http://www.gaussian.com/
[23] Coutinho J, Jones R, Briddon P R and Öberg S 2000 *Phys. Rev.* B **62** 10824
see also http://aimpro.ncl.ac.uk/
[24] Lewis J P, Glaesemann K R, Voth G A, Fritsch J, Demkov A A, Ortega J and Sankey O F 2001 *Phys. Rev.* B **64** 195103
see also http://www.hec.utah.edu/fireball/
[25] Ordejón P, Artacho E and Soler J M 1996 *Phys. Rev.* B **53** R10441
Soler J M, Artacho E, Gale J D, García A, Junquera J, Ordejón P and Sánchez-Portal D 2002 *J. Phys.: Condens. Matter* **14** 2745
see also http://www.uam.es/siesta/
[26] Goringe C M, Bowler D R and Hernández E 1997 *Rep. Prog. Phys.* **60** 1447
[27] Stillinger F H and Weber T A 1985 *Phys. Rev.* B **31** 5262
[28] Tersoff J 1986 *Phys. Rev. Lett.* **56** 632
Tersoff J 1988 *Phys. Rev.* B **37** 6991
Tersoff J 1988 *Phys. Rev.* B **38** 9902
[29] Brenner D W 1990 *Phys. Rev.* B **42** 9458
[30] Justo J F, Bazant M Z, Kaxiras E, Bulatov V V and Yip S 1998 *Phys. Rev.* B **58** 2539
[31] Tersoff J 1989 *Phys. Rev.* B **39** 5566
[32] Tersoff J 1988 *Phys. Rev. Lett.* **61** 2879
[33] Lii J-H and Allinger N L 1989 *J. Am. Chem. Soc.* **111** 8566
Lii J-H and Allinger N L 1989 *J. Am. Chem. Soc.* **111** 8576
Lii J-H and Allinger N L 1991 *J. Comput. Chem.* **12** 186
Lii J-H and Allinger N L 1998 *J. Comput. Chem.* **19** 1001
[34] Weiner P K and Kollman P A 1981 *J. Comput. Chem.* **2** 287
Weiner S J, Kollman P A, Case D A, Singh U C, Ghio C, Alagona G, Profeta S Jr and Weiner P K 1984 *J. Am. Chem. Soc.* **106** 765
Weiner S J, Kollman P A, Nguyen D T and Case D A 1986 *J. Comput. Chem.* **7** 230
Cornell W D, Cieplak P, Bayly C I, Gould I R, Merz K M Jr, Ferguson D M, Spellmeyer D C, Fox T, Caldwell J W and Kollman P A 1995 *J. Am. Chem. Soc.* **117** 5179
[35] Brooks B R, Bruccoleri R E, Olafson B D, States D J, Swaminathan S and Karplus M 1983 *J. Comput. Chem.* **4** 187
Momany F A and Rone R 1992 *J. Comput. Chem.* **13** 888
[36] http://www.omicron.de/index2.html/results/manipulation_on_the_atomic_scale/~Omicron
[37] Fotiadis D, Scheuring S, Müller S A, Engel A and Müller D J 2002 *Micron* **33** 327
[38] Thelander C and Samuelson L 2002 *Nanotechnology* **13** 108

[39] Loppacher C, Guggisberg M, Pfeiffer O, Meyer E, Bammerlin M, Luthi R, Schlittler R R, Gimzewski J K, Tang H and Joachim C 2003 *Phys. Rev. Lett.* **90** 066107
[40] Bouju X, Joachim C, Girard C and Sautet P 1993 *Phys. Rev.* B **47** 7454
[41] Girard C 1986 *J. Chem. Phys.* **85** 6750
[42] Buldum A and Ciraci S 1996 *Phys. Rev.* B **54** 2175
[43] Barker J A and Rettner C T 1992 *J. Chem. Phys.* **97** 5844
[44] Kürpick U and Rahman T S 1999 *Phys. Rev. Lett.* **83** 2765
[45] Daw M S, Foiles S M and Baskes M I 1993 *Mater. Sci. Rep.* **9** 251
[46] Voter A F and Chen S P 1986 *Proc. Mater. Res. Soc.* **82** 175
[47] Foiles S M, Baskes M I and Daw M S 1986 *Phys. Rev.* B **33** 7983
[48] Pizzagalli L and Baratoff A 2003 *Phys. Rev.* B **68** 115427
[49] Anderson A B and Hoffmann R 1974 *J. Chem. Phys.* **60** 4271
[50] Hoffmann R 1963 *J. Chem. Phys.* **39** 1397
[51] Tupper K J, Counts R W and Gajewski J J 1991 *Comput. Chem.* **15** 157
[52] Savary F, Weber J and Calzaferri G 1993 *J. Phys. Chem.* **97** 3722
[53] Sautet P and Joachim C 1991 *Chem. Phys. Lett.* **185** 23
[54] Bouju X, Joachim C and Girard C 1999 *Phys. Rev.* B **59** R7845
[55] Cerda J and Sautet P 1997 *Phys. Rev.* B **56** 15885
[56] Kühnle A, Meyer G, Hla S W and Rieder K H 2002 *Surf. Sci.* **499** 15
[57] Zeppenfeld P, Lutz C P and Eigler D M 1992 *Ultramicroscopy* **4244** 128
[58] Jung T A, Schlittler R R, Gimzewski J K, Tang H and Joachim C 1996 *Science* **271** 181
[59] Cuberes M T, Schlittler R R and Gimzewski J K 1996 *Appl. Phys. Lett.* **69** 3016
[60] Moresco F, Meyer G, Reider K H, Tang H, Gourdon A and Joachim C 2001 *Appl. Phys. Lett.* **78** 306
[61] Tang H, Cuberes M T, Joachim C and Gimzewski J K 1997 *Surf. Sci.* **386** 115
[62] Moresco F, Meyer G, Reider K H, Tang H, Gourdon A and Joachim C 2001 *Phys. Rev. Lett.* **87** 088302
[63] Allinger N L 1977 *J. Am. Chem. Soc.* **99** 8127
[64] Eigler D M, Lutz C P and Rudge W E 1991 *Nature* **352** 600
[65] Shen T C, Wang C, Abeln G C, Tucker J R, Lyding J W, Avouris Ph and Walkup R E 1995 *Science* **268** 1590
[66] Fishlock T W, Oral A, Egdell R G and Pethica J B 2000 *Nature* **404** 743
[67] Komeda T, Kim Y, Kawai M, Persson B N J and Ueba H 2002 *Science* **295** 2055
[68] Hansma P K 1977 *Phys. Rep.* **30** 145
[69] Wang W, Lee T and Reed M A 2004 *Nano Lett.* **4** 643
[70] Davis L C 1970 *Phys. Rev.* B **2** 1714
[71] Caroli C, Combescot R, Nozières P and Saint-James D 1972 *J. Phys. C: Solid State Phys.* **5** 21
[72] Persson B N J and Baratoff A 1987 *Phys. Rev. Lett.* **59** 339
[73] Lorente N and Persson M 2000 *Phys. Rev. Lett.* **85** 2997
[74] Lorente N 2004 *Appl. Phys.* A **78** 799
[75] Galperin M, Ratner M A and Nitzan A 2004 *J. Chem. Phys.* **121** 11965
[76] Pascual J I and Lorente N 2004 *Properties of Single Molecules on Crystal Surfaces* submitted
[77] Pascual J I, Jackiw J J, Song Z, Weiss P S, Conrad H and Rust H P 2001 *Phys. Rev. Lett.* **86** 1050
[78] Sainoo Y, Kim Y, Komeda T and Kawai M 2004 *J. Chem. Phys.* **120** 7249
[79] Agraït N, Untiedt C, Rubio-Bollinger G and Vieira S 2002 *Phys. Rev. Lett.* **88** 216803
[80] Agraït N, Untiedt C, Rubio-Bollinger G and Vieira S 2002 *Chem. Phys.* **281** 231
[81] Datta S 1995 *Electronic Transport in Mesoscopic Systems* (Cambridge: Cambridge University Press)
[82] Meir Y and Wingreen N S 1992 *Phys. Rev. Lett.* **68** 2512
[83] Haug H and Jauho A P 1996 *Quantum Kinetics in Transport and Optics of Semiconductors* (Berlin: Springer)
[84] Frederiksen T 2004 *Master Thesis* DTU, Lyngby
http://www.mic.dtu.dk/research/theoreticalnano/publications/theses.htm
[85] Frederiksen T, Brandbyge M, Lorente N and Jauho A P 2004 *Phys. Rev. Lett.* **93** 256601
[86] Bardeen J 1961 *Phys. Rev. Lett.* **6** 57
[87] Doyen G 1996 *Scanning Tunnelling Microscopy III* (*Springer Series in Surface Science*) ed R Wiesendanger and H J Güntherodt (Berlin: Springer)
Doyen G 1993 *J. Phys.: Condens. Matter* **5** 3305
[88] Tersoff J and Hamann D R 1983 *Phys. Rev. Lett.* **50** 1998
Tersoff J and Hamann D R 1985 *Phys. Rev.* B **31** 805
[89] Chen C J 1993 *Introduction to Scanning Tunneling Microscopy* (Oxford: Oxford University Press)
[90] Hofer W, Foster A S and Shluger A L 2003 *Rev. Mod. Phys.* **75** 1287
[91] Zawadowski A 1967 *Phys. Rev.* **163** 341

[92] Appelbaum J A and Brinkman W F 1969 *Phys. Rev.* **186** 464
[93] Pendry J B, Prêtre A B and Krutzen B C H 1991 *J. Phys.: Condens. Matter* **3** 4313
[94] Li J, Schneider W D, Berndt R, Bryant O and Crampin S 1998 *Phys. Rev. Lett.* **81** 4464
[95] Lorente N and Persson M 2000 *Faraday Discuss.* **117** 277
[96] Lorente N, Persson M, Lauhon L J and Ho W 2001 *Phys. Rev. Lett.* **86** 2593
[97] Lauhon L J and Ho W 1999 *Phys. Rev.* B **60** R8525
[98] Heinrich A J, Lutz C P, Gupta J A and Eigler D M 2002 *Science* **298** 1381
[99] Gao S, Persson M and Lundqvist B I 1992 *Solid State Commun.* **84** 271
Gao S, Persson M and Lundqvist B I 1993 *J. Electron Spectrosc. Relat. Phenom.* **64/65** 665
[100] Gao S, Persson M and Lundqvist B I 1997 *Phys. Rev.* B **55** 4825
[101] Walkup R E, Newns D M and Avouris Ph 1993 *Phys. Rev.* B **48** 1858
[102] Ho W 1996 *J. Phys. Chem.* **100** 13050
[103] Salam G P, Persson M and Palmer R E 1994 *Phys. Rev.* B **49** 10655
[104] Lorente N and Pascual J I 2004 *Phil. Trans. R. Soc.* **362** 1227
[105] Persson B N J and Ueba H 2002 *Surf. Sci.* **502/503** 18
[106] Gadzuk J W 1991 *Phys. Rev.* B **44** 13466
[107] Alavi S, Rousseau R and Seideman T 2000 *J. Chem. Phys.* **113** 4412
[108] Guo H, Saalfrank P and Seideman T 1999 *Prog. Surf. Sci.* **62** 239
[109] Alavi S, Rousseau R, Patitsas S N, Lopinksi G P, Wolkow R A and Seideman T 2000 *Phys. Rev. Lett.* **85** 5372
Alavi S, Rousseau R, Patitsas S N, Lopinksi G P, Wolkow R A and Seideman T 2000 *Faraday Discuss.* **117** 213
[110] Avouris Ph, Walkup R E, Rossi A R, Shen T C, Abeln G C, Tucker J R and Lyding J W 1996 *Chem. Phys. Lett.* **257** 148
[111] Hellsing B and Persson M 1984 *Phys. Scr.* **29** 360
[112] Head-Gordon M and Tully J C 1992 *Phys. Rev.* B **46** 1835
Head-Gordon M and Tully J C 1992 *J. Chem. Phys.* **96** 3939
[113] Bornscheuer K H, Nessler W, Binetti M, Hasselbrink E and Saalfrank P 1997 *Phys. Rev. Lett.* **78** 1174
[114] Runge E and Gross E K U 1984 *Phys. Rev. Lett.* **52** 997
[115] Rignanese G M, Blase X and Louie S G 2001 *Phys. Rev. Lett.* **86** 2110
[116] Lopinsky G P, Wayner D D M and Wolkow R A 2000 *Nature* **406** 44
[117] Asai Y 2004 *Phys. Rev. Lett.* **93** 246102
[118] Yu L H, Keane Z K, Ciszek J W, Cheng L, Stewart M P, Tour J M and Natelson D 2004 *Phys. Rev. Lett.* **93** 266802